Relaxation mechanisms in ultra-low damping Fe80Co20 thin films

Peer-reviewed author version

Rodriguez, DV; Gomez, JE; Alejandro, G; Felix, LA; VAN LANDEGHEM, Melissa; Goovaerts, E & Butera, A (2020) Relaxation mechanisms in ultra-low damping Fe80Co20 thin films. In: JOURNAL OF MAGNETISM AND MAGNETIC MATERIALS, 504 (Art N° 166692).

DOI: 10.1016/j.jmmm.2020.166692
Handle: http://hdl.handle.net/1942/33179

Journal Pre-proofs

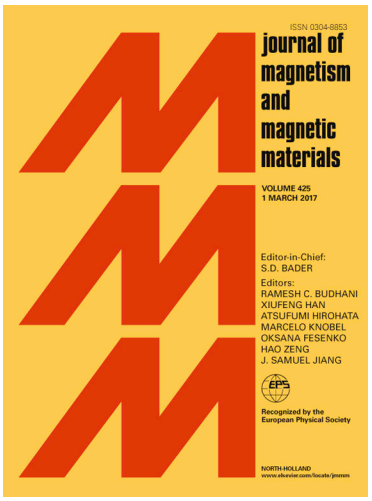

Relaxation mechanisms in ultra-low damping $Fe_{80}Co_{20}$ thin films

D. Velázquez Rodriguez, J.E. Gómez, G. Alejandro, L. Avilés Félix, M. van Landeghem, E. Goovaerts, A. Butera

PII: S0304-8853(20)30072-X
DOI: https://doi.org/10.1016/j.jmmm.2020.166692
Reference: MAGMA 166692

To appear in: *Journal of Magnetism and Magnetic Materials*

Received Date: 9 January 2020
Revised Date: 13 February 2020
Accepted Date: 29 February 2020

Please cite this article as: D. Velázquez Rodriguez, J.E. Gómez, G. Alejandro, L. Avilés Félix, M. van Landeghem, E. Goovaerts, A. Butera, Relaxation mechanisms in ultra-low damping $Fe_{80}Co_{20}$ thin films, *Journal of Magnetism and Magnetic Materials* (2020), doi: https://doi.org/10.1016/j.jmmm.2020.166692

Relaxation mechanisms in ultra-low damping $Fe_{80}Co_{20}$ thin films.

D. Velázquez Rodriguez [1, *], **J. E. Gómez** [1], **G. Alejandro** [1], **L. Avilés Félix** [2], **M. van Landeghem** [3], **E. Goovaerts** [3] **and A. Butera** [4]

(1) Centro Atómico Bariloche. Comisión Nacional de Energía Atómica (CNEA). Consejo Nacional de Investigaciones Científicas y Técnicas (CONICET). Av. Bustillo 9500, 8400 Bariloche, Río Negro, Argentina.
(2) Spintec, Université Grenoble Alpes, CNRS, CEA, Grenoble INP, IRIG-SPINTEC, 38054 Grenoble, France.
(3) Departement Fysica, Universiteit Antwerpen, Groenenborgerlaan 171, B-2020 Antwerpen, Belgium.
(4) Centro Atómico Bariloche. Comisión Nacional de Energía Atómica (CNEA). Consejo Nacional de Investigaciones Científicas y Técnicas (CONICET). Universidad Nacional de Cuyo (UNCUYO). Av. Bustillo 9500, 8400 Bariloche, Río Negro, Argentina.

Abstract

Ferromagnetic thin films with ultra-low damping constants (α) are intensively studied for applications in spintronic devices. We report here the influence of the sputtering conditions (deposition power and temperature) on the magnetic properties of $Fe_{80}Co_{20}$/Ta bilayers deposited on MgO (001) and Si (001) which have been studied using ferromagnetic resonance (FMR) and magneto-optic Kerr-effect (MOKE) techniques. We have found that for the studied fabrication conditions the samples deposited on MgO(001) have [100] epitaxial growth with a cubic anisotropy field H_c~300 Oe, while those sputtered on Si(001) grow polycrystalline with a small uniaxial anisotropy due to the deposition conditions. With measurements at different excitation frequencies we have determined exceptionally low damping values for ferromagnetic conductors (α~ $3x10^{-3}$), which makes the $Fe_{80}Co_{20}$/Ta system an excellent candidate for future applications in spintronic devices. From the analysis of the dependence of the FMR linewidth on the orientation of the applied magnetic field and the excitation frequency in FMR experiments, we were able to separate the contribution of the different relaxation mechanisms (Gilbert damping, two magnon scattering and mosaicity) to the linewidth and to explain quantitatively the observed behavior.

(*) Author to whom correspondence should be addressed: daniel.velazquez@cab.cnea.gov.ar

Introduction

FeCo alloys have been widely studied for decades because of their unique metallic and magnetic properties. In recent years the search of new systems adequate for spintronic devices promoted the study of bilayers constituted by a ferromagnetic film in contact with a non-magnetic conductive metal (NM) (Ta, W, Os, Pt, Au, etc.). In these bilayers when the FM is exposed to microwave radiation it can be driven to its ferromagnetic resonance (FMR) condition to produce the injection of a pure spin current through the FM/NM interface. In this phenomenon, known as spin pumping [**1-3**], a pure spin current is the result of an additional relaxation mechanism that appears in the bilayer mediated by the NM conduction electrons. The search for new materials and alloys suitable for the fabrication of these bilayers, from which an intense pure spin current could be obtained, is one of the challenges of today's spintronic [**4**]. The intensity of the pure spin current density, $J^0_s{}^{(sp)}$, arising from the spin pumping phenomenon is inversely proportional to the damping parameter (α) of the ferromagnet ($J^0_s{}^{(sp)} \propto 1/\alpha^2$)[**5**], which motivated the search of materials with very low damping constants.

The phenomenological parameter α contains all the information about the different mechanisms that contribute to relax the magnetization of the FM layer to the equilibrium configuration. Theoretically, several models try to explain the underlying physics of this parameter. Brataas *et al.* [**6**] and Liu *et al.* [**7**] used the scattering theory to describe the damping. Damping results from scattering of the conducting spin polarized electrons with the magnetization according to the s-d scattering model are given in Ref. [**8**]. Other damping mechanisms, which take into account the electron-electron and electron-impurity scattering are discussed in Ref. [**9**]. Experimentally, the parameter α can be determined from FMR linewidth measurements (ΔH_r) at different excitation frequencies ($\omega/2\pi$). For the determination of α it is assumed that the relation ΔH_r vs. ω is linear, which, in general, is only valid for intrinsic relaxation mechanisms [**10**]. In some cases the dependence of ΔH_r on the excitation frequency is not linear due to, for example, the two magnon scattering mechanism [**11-13**]. This mechanism provides a non-linear extrinsic contribution to ΔH_r, which should be included for the correct determination of the damping parameter. A recent work by M. Schoen *et al.* [**14**] reported that FeCo polycrystalline alloys present an ultra-low magnetic damping near the $Fe_{75}Co_{25}$ concentration (ΔH_r~20 Oe at 10 GHz), which makes it a promising candidate for the efficient injection of spin currents.

In this work we carried out an experimental study of the structural and magnetic properties of $Fe_{80}Co_{20}$/Ta bilayers with the purpose of studying how the variation of the growing parameters: sputtering power and temperature, amorphous or single crystal substrates, affects the magnetic properties of the alloy and finding the optimal fabrication conditions that reduce the linewidth as much as possible.

Experimental details

The samples were deposited by dc magnetron sputtering at an Ar pressure of 1.8 mTorr. We used an alloyed $Fe_{80}Co_{20}$ target (38 mm diameter) with a substrate to target distance of 7.5 cm. The base pressure before depositing the bilayers was $\lesssim 10^{-6}$ Torr. The bilayers are of the form [MgO (001) or Si (001)]/$Fe_{80}Co_{20}$ (10 nm)/Ta (5 nm). In order to find the optimal deposition conditions, different series of films were deposited by varying the sputtering power (13 W, 16 W and 20 W which are equivalent to power densities of 1.15

W/cm^2, 1.41 W/cm^2 and 1.76 W/cm^2, respectively), the substrate used (MgO (001) single crystals or (001) Si wafers with a natural oxide amorphous surface layer) and the temperature of the substrate before deposition (20 ºC and 150 °C) maintaining a fixed power (20 W). Films deposited on MgO and Si were grown simultaneously. Table I shows the fabrication conditions of the eight samples studied in this work. The sputtering rate of $Fe_{80}Co_{20}$ for 13 W, 16 W and 20 W was 0.06 nm/s, 0.075 nm/s and 0.093 nm/s, respectively. The Ta capping layer was deposited at a power of 20 W with a sputtering rate of 0.13 nm/s and at a fixed temperature of 20 ºC for all the samples.

Table I. Detail of the fabrication conditions of the eight samples deposited on Si and MgO. All samples have a thickness of 10 nm ($Fe_{80}Co_{20}$)/ 5 nm (Ta).

Sample name		Sputtering power and temperature
13W-Si	13W-MgO	13 W-20 ºC
16W-Si	16W-MgO	16 W-20 ºC
20W-Si	20W-MgO	20 W-20 ºC
150C-Si	150C-MgO	20 W-150 ºC

The magnetic characterization was performed by using a vibrating sample magnetometer (VSM) and a magneto-optic Kerr-effect (MOKE) magnetometer to determine dc magnetization values and the behavior of the *M* vs. *H* hysteresis loops. FMR measurements using X, K, Q, and W-bands (9.8, 24, 35 and 94 GHz) were performed to study the dynamic response. The FMR measurements were conducted using the commercial Bruker spectrometers ESP300 (X, K, and Q-bands) and Elexsys E680 (W-band). Samples were placed in the center of a resonant cavity whose dimensions are characteristic of the microwave frequency band (X, K, Q, or W). The dc magnetic field was applied (in most cases) in the direction parallel to the plane of the film and the microwave field perpendicular to the sample. The films could be rotated with respect to the applied field in order to determine the angular dependence of the resonance field and the linewidth. To improve the signal to noise ratio, standard field modulation and lock-in detection techniques were employed.

Results and Discussion

1.*MOKE and VSM measurements.*

Fig. 1 shows the normalized hysteresis loops obtained in the longitudinal MOKE setup (the magnetization is contained in the optic plane) for different orientations of the in-plane (IP) applied field $\boldsymbol{H}$, expressed by the angle φ_H between $\boldsymbol{H}$ and the [100] substrate direction. The samples deposited on Si (Fig. 1(a-d)) have a similar behavior in terms of remanence, which is compatible with a weak uniaxial symmetry. Given the small angular changes in the hysteresis loops, it is expected that this anisotropy has a relatively small value ($\lesssim$ 10 Oe). For the three deposition powers under study the value of the coercive

field is similar (H_c~45 Oe), being considerably smaller in the sample deposited at 150 °C (H_c~24 Oe).

Fig. 1(e-h) shows the hysteresis loops of the samples deposited on MgO. The remanence values at different angles display a maximum and minimum every 45° which is distinctive of a cubic fourfold symmetry and suggests an epitaxial film growth. Note that the remanence is maximum for φ_H = 45º and 135º which is a strong indication that the FeCo <100> easy axes are rotated by 45º with respect to the MgO substrate. The H_c values are similar for the samples deposited at 13 W, 16 W and 150 ºC on the MgO substrates. This evidences that the effect of temperature and/or low sputtering power helps Fe and Co atoms to better match the MgO substrate during the deposition and grow a film with fewer defects and pinning sites. On the other hand, the sample deposited at 20 W still preserves the fourfold symmetry but it shows a broader hysteresis loop with a larger H_c value, which is consistent with the fact that an increase in the deposition rate produces a more disordered film. The differences in the shape of the hysteresis loops in the H_c region, that are observed particularly in Fig. 1(f), have been extensively discussed in terms of magnetization reversal processes in systems with mixed uniaxial (K_u) and cubic (K_c) anisotropies [**15-19**]. In these works [**15-19**] the authors reported hysteresis loops with multi-jumps that depend on the competition between uniaxial and cubic anisotropies and the relative orientation of the principal anisotropy axes. When the easy axis of K_u is parallel to one of the K_c easy axes, the K_u hard axis lies along the perpendicular K_c easy axis, so that K_c axis 90º apart are not equivalent. In Ref. [**17**] it is argued that for systems where $K_u << K_c$ and the easy uniaxial axis is aligned with one of the easy cubic axes (easy-easy), the hysteresis loops have a square shape in the direction in which the easy axes of both anisotropies coincide and a loop with a 2-jump switching in the direction in which the hard uniaxial axis is parallel to the easy cubic axis (hard-easy). When the applied field is along the easy-easy direction the reversion process occurs through the nucleation of 180º domain walls, while for the applied field along the hard-easy direction the reversion process occurs through the successive nucleation of two 90º domain walls [**17**]. This difference in the reversal process between the FeCo easy cubic directions [100] and [010] can be the reason for the differences between the hysteresis loops at φ_H = 45º ($\boldsymbol{H} \parallel [100]_{FeCo}$) and φ_H = 135º ($\boldsymbol{H} \parallel [010]_{FeCo}$) in the samples deposited on MgO, especially in Fig. 1(f).

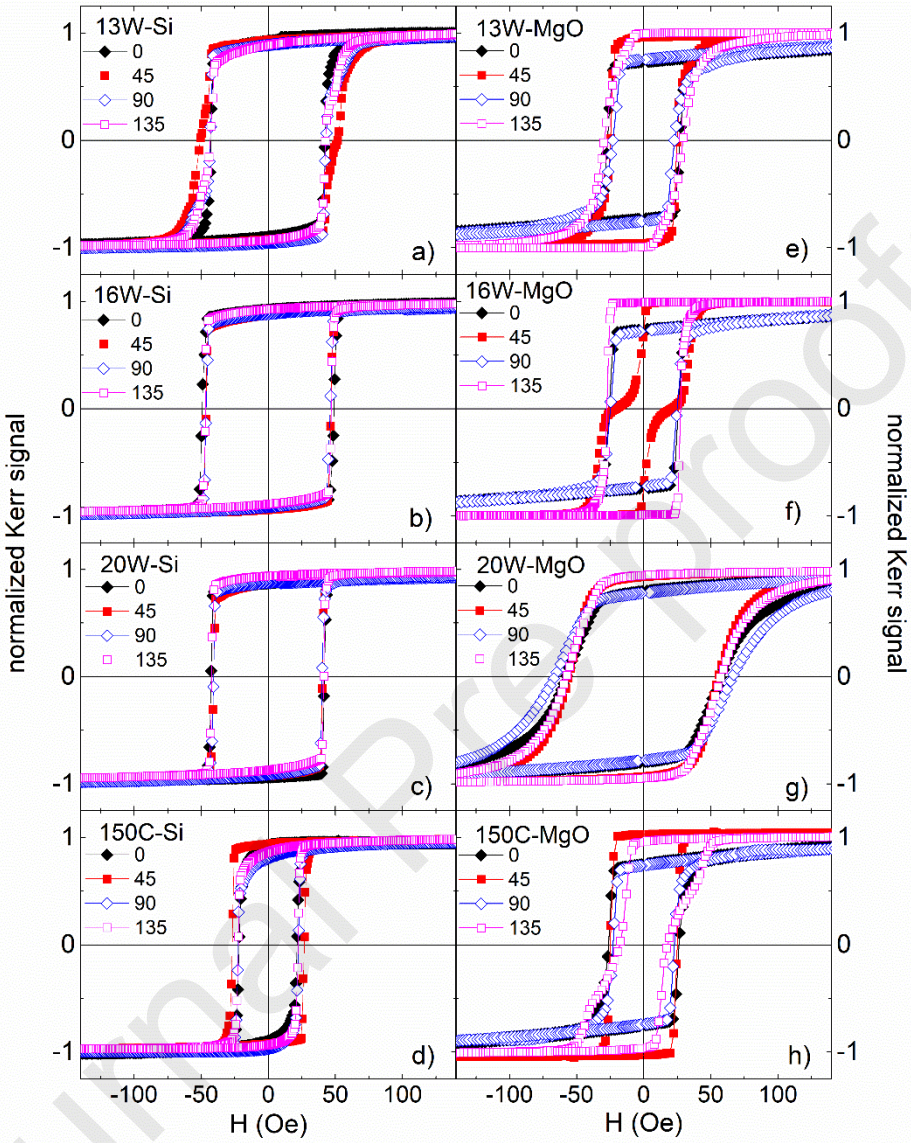

Fig 1. In-plane hysteresis loops measured using the MOKE technique for different orientations of the in-plane applied field with respect to the substrate [100] direction. Magnetization data were normalized to the value of M for H=1 kOe.

According to the phenomenological model of [**17**] the sample 16W-MgO (Fig. 1(f)) is expected to present the highest value of K_u/K_c since it has a more pronounced 2-jump hysteresis loop. Likewise, the sample 20W-MgO (Fig. 1(g)) is expected to present the lowest value of K_u/K_c. The precise determination of the anisotropy constants K_u and K_c will be discussed in the next section through FMR measurements.

The saturation magnetization of all the samples under study was determined by VSM measurements. The values obtained are presented in Table. II.

Table II. M_S values determined from VSM measurements.

Substrate / Power and temperature	Si M_s (emu/cm^3)	MgO M_s (emu/cm^3)
13 W-20 ºC	1700 (100)	1700 (100)
16 W-20 ºC	1750 (100)	1750 (100)
20 W-20 ºC	1850 (100)	1800 (100)
20 W-150 ºC	1700 (100)	1600 (100)

The average value of M_s obtained for the eight films (M_s=1730 $\pm$ 80 emu/cm^3) is about 10% lower than that of the bulk material (M_s=1900 emu/cm^3 for $Fe_{80}Co_{20}$) [**20**]. This may be due to the formation of an interfacial dead layer [**21**] or a small amount of residual oxygen in the sputtering chamber [**22**].

2. *FMR measurements and analysis.*

The classical Landau-Lifshitz-Gilbert equation of motion is generally used to describe the dynamics of the magnetization vector:

$$\frac{d\boldsymbol{M}}{dt} = -\gamma \boldsymbol{M} \times \left(\boldsymbol{H}_t - \frac{\alpha \, d\boldsymbol{M}}{\gamma M \, dt} \right), \qquad (1)$$

where α is the damping parameter, $\gamma = \frac{g\mu_\beta}{\hbar}$ is the gyromagnetic factor, $\boldsymbol{M}$ the magnetization vector, and $\boldsymbol{H}_t$ is the total magnetic field (that includes the external field and contributions arising from anisotropies). Using the formalism of Smit and Beljers [**23**] Eq. (1) can be solved for the uniform mode of precession. To obtain the dispersion relation when $\boldsymbol{H}$ is applied parallel to the (001) film plane we propose a magnetic free energy of the form:

$$F(\theta,\varphi) = -MH\sin\theta\cos(\varphi - \varphi_H) + 2\pi M^2\cos^2\theta - K_u\sin^2\theta\cos^2(\varphi - \pi/4) - K_c\left(\frac{\sin^2 2\theta + \sin^2 2\varphi \sin^4\theta}{4}\right), \qquad (2)$$

where we consider the Zeeman energy of the magnetization $\boldsymbol{M}$ in an external field $\boldsymbol{H}$, characterized by an in-plane angle φ_H, (first term in Eq. (2)), the shape energy given by the demagnetization factor of a thin film (second term in Eq. (2)), and the uniaxial and cubic energies characterized by the anisotropy constants of uniaxial and cubic symmetry K_u and K_c, respectively (third and fourth terms in Eq. (2)). φ is the azimuthal angle that forms the projection of $\boldsymbol{M}$ with the spherical coordinate system ($\varphi = 0$ corresponding to the MgO [100] direction), and θ is the out of plane polar angle. Substituting Eq. (2) in the Smit and Beljers equation for the dispersion relation:

$$\left(\frac{\omega}{\gamma}\right)^2 = \frac{1}{M^2\sin^2\theta}\left(F_{\theta\theta}F_{\varphi\varphi} - F_{\varphi\theta}^2\right), \qquad (3)$$

we obtain the dispersion relation for our system when the field H is applied in the film plane:

$$\left(\frac{\omega}{\gamma}\right)^2 = \left[H\cos(\varphi-\varphi_H) + H_u\cos^2(\varphi-\pi/4) - H_c\left(1-\frac{\sin^2 2\varphi}{2}\right) + 4\pi M_s\right] \left[H\cos(\varphi-\varphi_H) + H_u\cos 2(\varphi-\pi/4) + H_c\cos 4\varphi\right]. \quad (4)$$

In Eq. (3) it is assumed that $|\boldsymbol{M}| = M_s$. $F_{\theta\theta}$, $F_{\varphi\varphi}$ and $F_{\varphi\theta}$ represent the second partial derivatives of the free energy with respect to the spherical angles and $\omega/2\pi$ is the excitation frequency. In Eq. (4), H_u and H_c are the uniaxial and cubic anisotropy fields defined as $H_u = 2K_u/M$ and $H_c = 2K_c/M$, respectively.

FMR spectra collected for the in-plane angular variation of the applied magnetic field for the 150C-MgO sample in X-band (9.8 GHz) are shown in Fig. 2, where the fourfold symmetry can be clearly observed. From these, and other similar spectra, we obtained the angular dependence of the resonance field and the linewidth for two excitation frequencies (X and K-bands) for the samples deposited on MgO, as shown in Fig. 3. Eq. (4) was used to fit the in-plane angular variation of the resonance field with the same set of parameters for both frequencies.

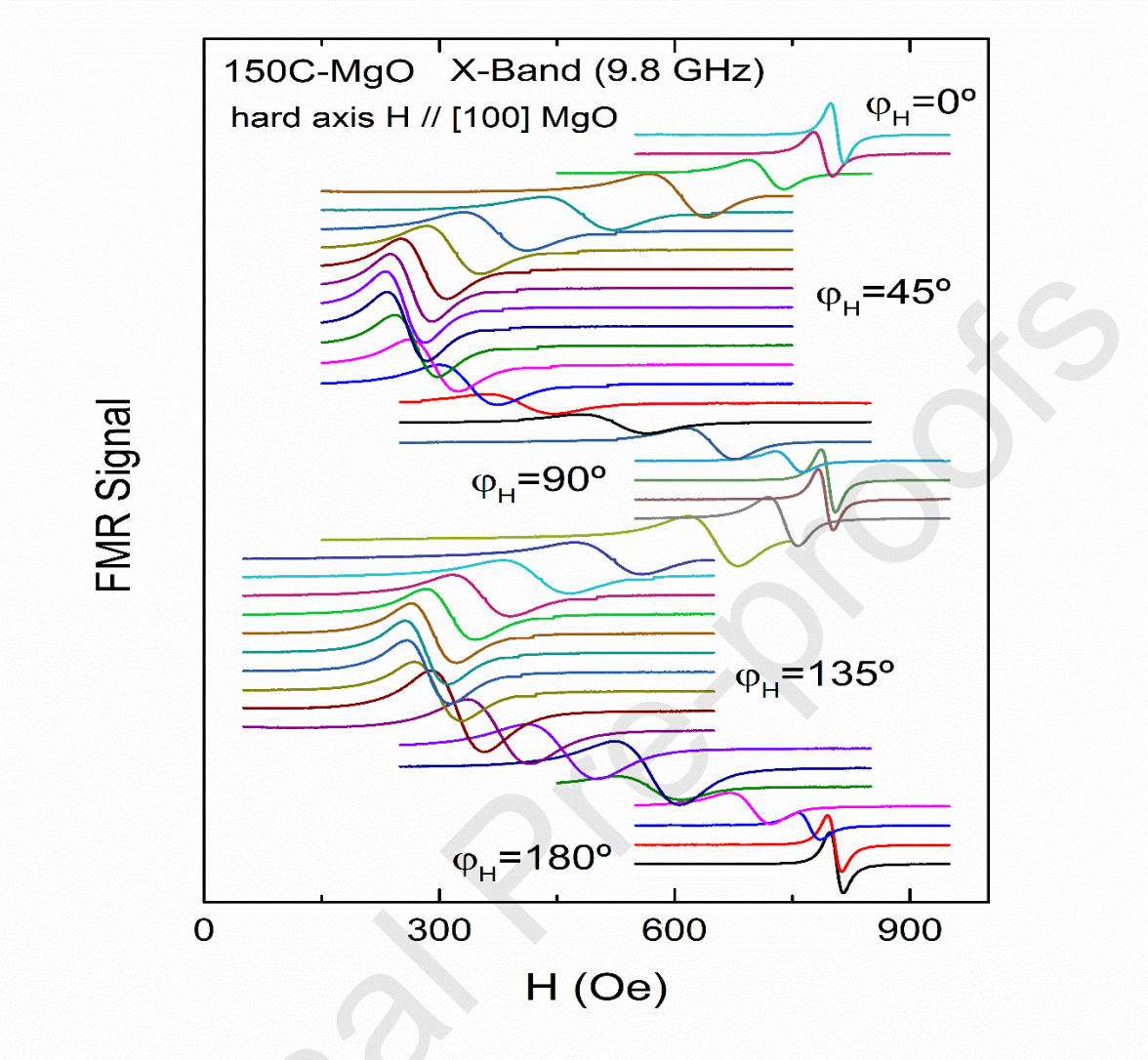

Fig. 2. X-band (9.8 GHz) FMR spectra collected for the in-plane angular variation of the applied magnetic field for the 150C-MgO sample.

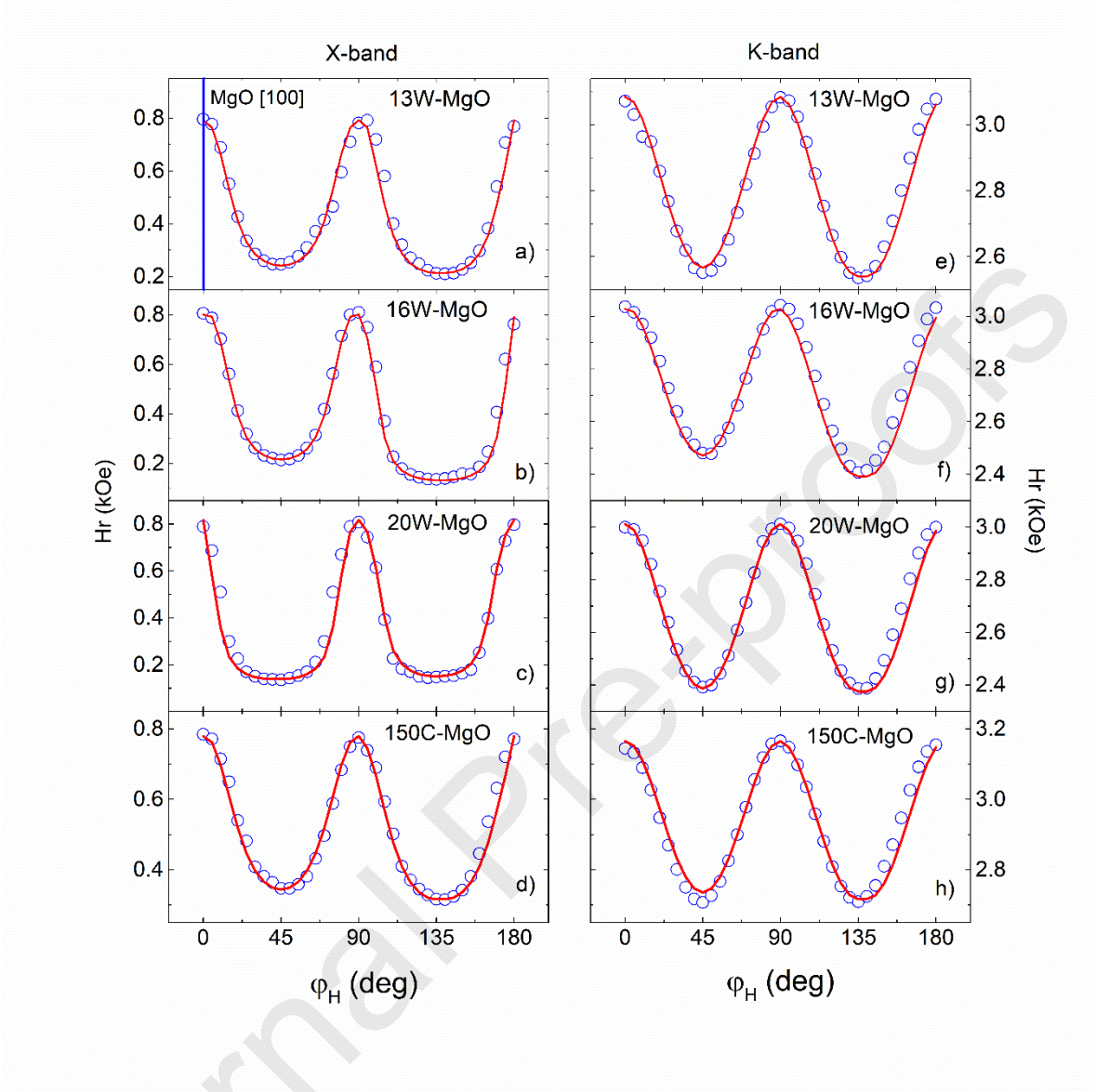

Fig. 3. In-plane angular variation of the resonance field (open circles) for the films deposited on MgO measured at X- and K- bands with the corresponding fit (solid line) obtained from Eq. (4). The vertical solid line in panel a) indicates the MgO [100] crystalline direction.

For the fit we used the M_s values presented in Table II. The value of φ was numerically calculated for each value of H and φ_H by minimizing Eq. (2) for $\theta = \pi/2$ (in-plane configuration). From the best fit that simultaneously describes the angular variation of H_r at both frequencies we obtained the values of H_u and H_c, which are shown in Table III, together with the parameters obtained for the samples deposited on Si. With the same H_u and H_c values obtained for the 150C-MgO sample at low frequencies, we also fitted the FMR W-band angular variation (see Fig. S3(a) supplemental material). The value of $g = 2.08(1)$, used to estimate the parameters shown in Table III, was obtained from W-band resonance field data parallel and perpendicular to the film plane, which are consistent with values reported in other Fe-rich alloys [**24, 25, 27**]. The good fitting for

different excitation frequencies with a single set of parameters supports the validity of the proposed model.

Table. III. Values of H_u , H_c and K_u/K_c obtained from the fit of the in-plane resonance field using Eq. (4).

sample	Si	MgO		
	H_u (Oe)	H_u (Oe)	H_c (Oe)	K_u/K_c (%)
13W	5 (1)	12 (2)	290 (10)	4
16W	10 (1)	42 (5)	320 (20)	13
20W	8 (1)	6 (1)	340 (20)	2
150C	10 (1)	11 (2)	230 (10)	5

The samples deposited on Si present only a relatively small uniaxial anisotropy field (H_u ~ 5-10 Oe), which is consistent with the MOKE measurements analyzed in the previous section, and is usually observed in sputtered films due to residual stresses or oblique sputtering [**26**]. This uniaxial anisotropy, with the same order of magnitude, is also observed in the samples deposited on MgO. The films grown on MgO, however, present a much larger magnetocrystalline cubic anisotropy, as can be seen from the in-plane angular variation of the resonance field (Fig. 3(a-h)). The values of the cubic anisotropy field obtained from the fit (H_c ~300 Oe) are of the order, but somewhat smaller, than those reported in bulk FeCo alloys (H_c ~400 Oe) [**20**]. Note also that, as already observed in the MOKE hysteresis loops, the [100] cubic easy axis of $Fe_{80}Co_{20}$ is rotated by 45º with respect to the [100] direction of the MgO substrate. In order to verify the $Fe_{80}Co_{20}$ epitaxy on the MgO (001) crystal we acquired x-ray $\theta - 2\theta$ diffractograms and phi-scan measurements on a thicker film (80 nm) deposited under similar sputtering conditions (15 W, 150 ºC). Results are presented in Figs. S1 and S2 of the supplemental material. With these data we validated the single crystal nature of the film and the 45º rotation of the [100] $Fe_{80}Co_{20}$ crystal direction with respect to the MgO substrate. On the other hand, the uniaxial easy axis is parallel to one of the cubic easy axis, in accordance with what was assumed in the previous section, where the appearance of multi-jumps in the hysteresis loop is determined by the magnitude of K_u/K_c. The value of this ratio is given in Table III, where we can see that the sample that presents a hysteresis loop with two well defined jumps (Fig. 1(f)) is the one with the highest value of K_u/K_c. The rest of the films have considerably smaller values of K_u/K_c with cubic easy axis M vs. H loops that tend to be more similar.

From the FMR linewidth measured at different excitation frequencies, we can estimate the damping parameter α. The dependence of ΔH_r with ω is usually assumed as linear and is given by Eq. (5) [**5**,**10**]:

$$\Delta H_r = \frac{2}{\sqrt{3}}\alpha\frac{\omega}{\gamma} + \Delta H_0 \,. \qquad (5)$$

Eq. (5) has a frequency dependent term that describes the intrinsic contribution to the linewidth, while it is assumed that all extrinsic contributions are frequency independent and are accounted for by the value of the inhomogeneous linewidth ΔH_0. This term is originated in the distribution of anisotropies that is characteristic of the growing process. In this equation ΔH_r is the total peak-to-peak linewidth. The factor $2/\sqrt{3}$ is given by the

difference between the peak-to-peak linewidth in the derivative of the Lorentzian function (line profile in our FMR experiments) and the full width at half maximum (FWHM) of the Lorentzian absorption. In Fig. 4(a) we show the dependence of the linewidth as a function of frequency for the sample 150C-MgO for the in-plane easy and hard directions (solid symbols) and the corresponding fit (solid line) for the hard axis data, which is found to be linear. A linear fit for the easy axis data is also shown (dotted line). The clear nonlinear behavior along the easy direction (solid squares) will be discussed later.

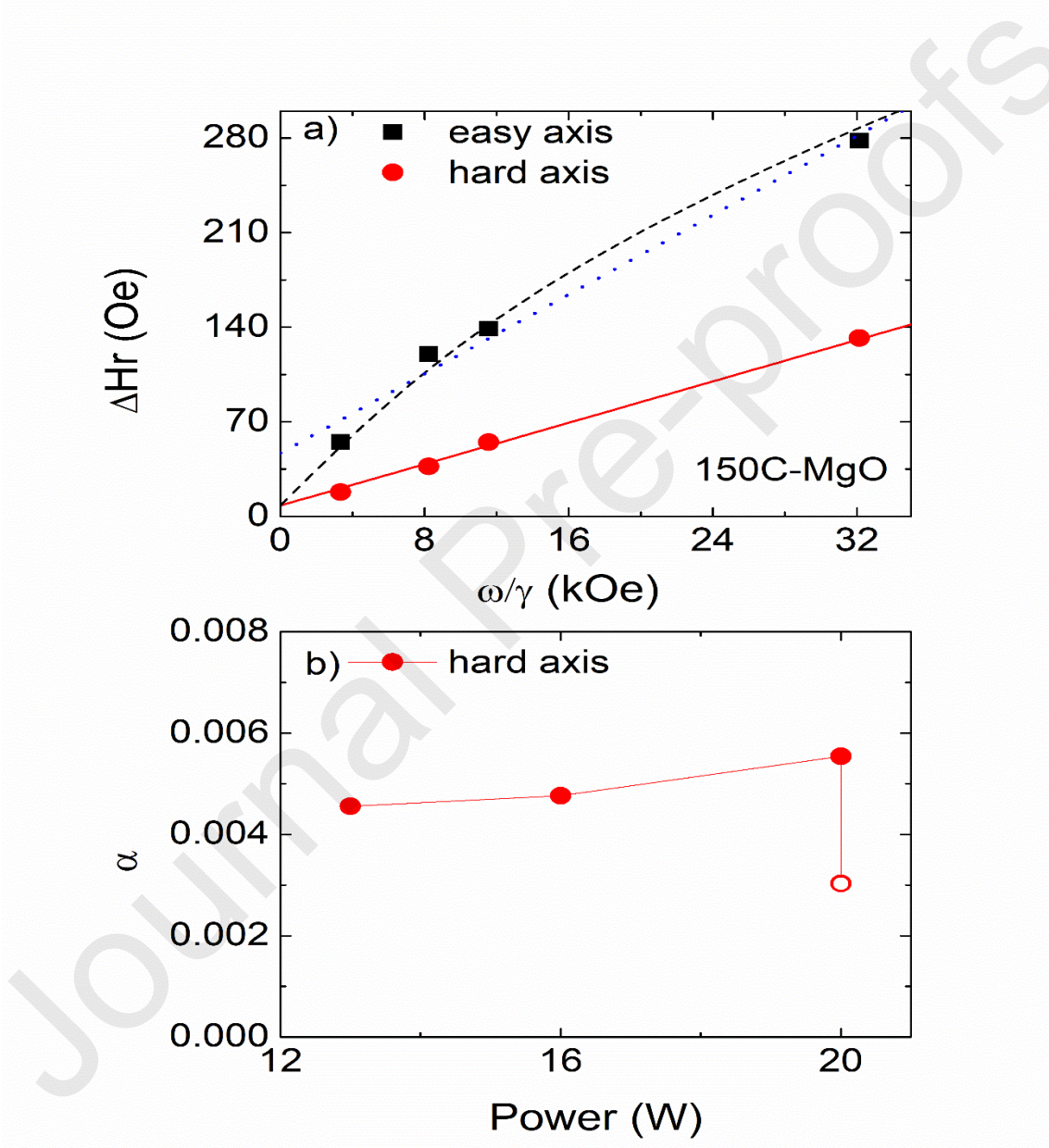

Fig.4. a) Frequency dependence of the resonance linewidth for the sample 150C-MgO for the easy (solid squares) and hard (solid circles) directions. The fits were made considering a linear dependence given by Eq. (5) for the hard (solid line) and easy (dotted line) directions, while the dashed line represents the linear contribution given by Eq. (5) for the hard direction with the addition of a term calculated from Eq. (6). **b)** Damping parameter, α, obtained from the linear fit of the data points of Fig. 4(a) for the hard direction (solid

circles) for the three samples deposited on MgO at room temperature and for the sample deposited at 150º C (open symbols).

The values of α obtained from Eq. (5) for the samples deposited on MgO (Fig. 4(b)) show that for powers of 12 and 16 W almost no differences are observed. For 20 W there is an increase in α that can be reduced if the deposition temperature is raised to 150 ºC. This suggests that the most favorable conditions to obtain samples with small damping, $\alpha \sim 3 \times 10^{-3}$, (usually $\alpha \sim 10^{-2}$ [**27**] for ferromagnetic conductors) could be sputtering power ~16 W and 150 °C of deposition temperature. All samples deposited on Si showed large damping values of ($\alpha \gtrsim 10^{-2}$) compared to the samples deposited on MgO. Since the main goal of this work is to obtain samples with small α ($\leq 10^{-3}$) from now on we will make a detailed analysis of the behavior of the linewidth for the samples deposited on MgO. From the linear fits we also obtained $\Delta H_0 \sim 8$ Oe for the different films, which shows the relatively good quality of the deposited samples. Recent published results [**14, 28, 29, 30**] of low damping constants in ferrous metallic alloy films report α values similar to our estimations made in $Fe_{80}Co_{20}$. However, in these references, the reported value of α was estimated after subtracting other relaxation mechanisms that contribute to total effective damping (called α_{SP} and α_{rad}). The spin pumping contribution α_{SP} is a consequence of an additional interfacial relaxation process, mediated by the conduction electrons of the normal metal (Ta in our case). The necessary thickness dependence of the FM layer to determine this contribution was not carried out in this work ($\alpha_{SP} \propto \left(\frac{1}{t_{FM}}\right)$, where t_{FM} is the thickness of the ferromagnetic layer). In any case, the value of α obtained in our study is an upper limit for the Gilbert damping constant of $Fe_{80}Co_{20}$/Ta bilayers. The radiative damping contribution (α_{rad}) is subtracted when a coplanar waveguide (CPW) is used for FMR measurements. Our measurements were made using a resonant cavity which ensures that all microwave energy is absorbed into the cavity. Therefore, it is not necessary to take this term into account in our analysis.

If we assume a linear frequency dependence of the linewidth for the easy in-plane magnetization direction (dotted line in Fig. 4(a)), we obtain an α parameter that duplicates that obtained for the hard in-plane magnetization direction. In Refs. [**27, 31, 32**] it is mentioned that the α parameter can be anisotropic, however the reported increase is $\Delta\alpha/\alpha$ ~15% [**27**]. In our case we have a much larger difference, which is a strong indication that Eq. (5) is not enough to satisfactorily describe the system under study. This suggests that when the field is applied along the direction of easy magnetization we have an additional non-linear extrinsic relaxation mechanism, so the ΔH_r is larger in that direction. This change in the mechanism of relaxation between the easy [100] and hard [110] film directions was previously reported in systems with cubic magnetocrystalline anisotropy [**13, 33**] and was ascribed to two magnon scattering (ΔH_{2M}). This contribution is known to depend on the direction of the applied field, being maximum for $\boldsymbol{H}$ || $[100]_{FeCo}$ (film easy axis) [**11-13**] and minimum for $\boldsymbol{H}$ || $[110]_{FeCo}$ (film hard axis) [**13, 31**]. The angular and frequency dependence is generally described by the following formula [**13, 33**]:

$$\Delta H_{2M}(\omega,\varphi_H) = \Gamma\, f(\varphi_H)\, \sin^{-1}\left[\sqrt{\frac{\sqrt{\omega^2 + \left(\omega_0/2\right)^2} - \omega_0/2}{\sqrt{\omega^2 + \left(\omega_0/2\right)^2} + \omega_0/2}}\right] U(\theta_H), \qquad (6)$$

where $\omega_0 = \gamma H_{eff} = \gamma(4\pi M_{eff})$, H_{eff} is the effective anisotropy field, and M_{eff} is the effective magnetization. The factor Γ is the strength of the two magnon scattering, and the function $f(\varphi_H)$ gives the behavior of ΔH_{2M} according to the direction of $\boldsymbol{H}$ with respect to the principal in-plane crystallographic direction. The function $U(\theta_H)$ describes the fact that ΔH_{2M} is zero when the external field is applied perpendicular ($U(\theta_H = 0) = 0$) and maximum when it is parallel to the plane of the film ($U(\theta_H = \pi/2) = 1$) [**11-13**]. It has been extensively reported that the two magnon scattering mechanism occurs when magnetic inhomogeneities generate scattering of the uniform mode (with wave vector $\boldsymbol{k} = 0$) into nonuniform modes ($\boldsymbol{k} \neq 0$) [**11-13**]. In our case the magnetic inhomogeneities will be treated as lattice defects, so it is expected that the in-plane angular dependence of ΔH_{2M} reflects the lattice symmetry. Given the cubic symmetry presented by the samples under study and following [**11**], the angular dependence that describes a fourfold symmetry is given by $f(\varphi_H) = \sin^2(2\varphi_H)$. The dashed line in Fig. 4(a) shows the added contributions deduced from Eqs. (5) and (6) using the estimated M_s (Table II) and α (Table IV) parameters for this sample. The parameter Γ in Eq. (6) was left free in order to achieve a rough estimate since for the realization of a better fit we would have needed additional experimental data as a function of frequency. We estimated $\Gamma = 195\ (20)$ Oe, which is consistent with values reported in Fe based multilayers [**33**].

Considering the contributions from Eqs. (5) and (6) to ΔH_r is not enough to explain the behavior of the in-plane angular variation of ΔH_r. Because real samples are not an array of perfectly aligned cubic crystals, the principal crystallographic directions may be misaligned in different crystals, but this misalignment has to be small ($< 5^\circ$) or the cubic symmetry would be gradually lost in the macroscopic sample. This leads to the detected FMR signal being an average of FMR lines with different H_r and in consequence, a broadening of ΔH_r occurs. This contribution, which scales approximately as $\frac{\partial H_r}{\partial \varphi_H}$, is usually called mosaicity and was estimated by using computer simulations. To simplify the simulations we considered that there is only mosaicity in the plane of the film. We introduce the mosaicity by making the substitution $\varphi = \varphi + \varphi_m$ in Eq. (2), where the probability of finding φ_m is given by a Gaussian distribution with zero mean and $\Delta\varphi_m^2$ variance. For each value of φ_m we calculated the corresponding value of H_r and generated a FMR Lorentzian line with intrinsic resonance linewidth, $\Delta H_r = \frac{2}{\sqrt{3}}\alpha\frac{\omega}{\gamma}$. In each simulation we generated 1000 FMR lines (above this number we did not observe significant changes in the simulated line) that were averaged to calculate the contribution of mosaicity to ΔH_r. Fig. 5 shows the measured values of ΔH_r (solid circles) and the added contributions of ΔH_{2M} and mosaicity (solid line) for two excitation frequencies (X-band and K-band). In the panel corresponding to the 150C-MgO sample for X-band these contributions are also shown separately, mosaicity (dashed line) and ΔH_{2M} (dotted line). Table IV presents the values of α obtained from the linear fit of the frequency dependence of ΔH_r for the hard direction with Eq. (5) (Fig. 4(b)) and the simulated parameters $\Delta\varphi_m$ (mosaicity) and $\Gamma^\omega = \Gamma \sin^{-1}\sqrt{\frac{\sqrt{\omega^2 + (\omega_0/2)^2} - \omega_0/2}{\sqrt{\omega^2 + (\omega_0/2)^2} + \omega_0/2}}$. For this simulation we used the values of M_s, H_u and H_c that were obtained from the VSM measurements and from the fitting of the in-plane angular variation of the experimental resonance fields, respectively.

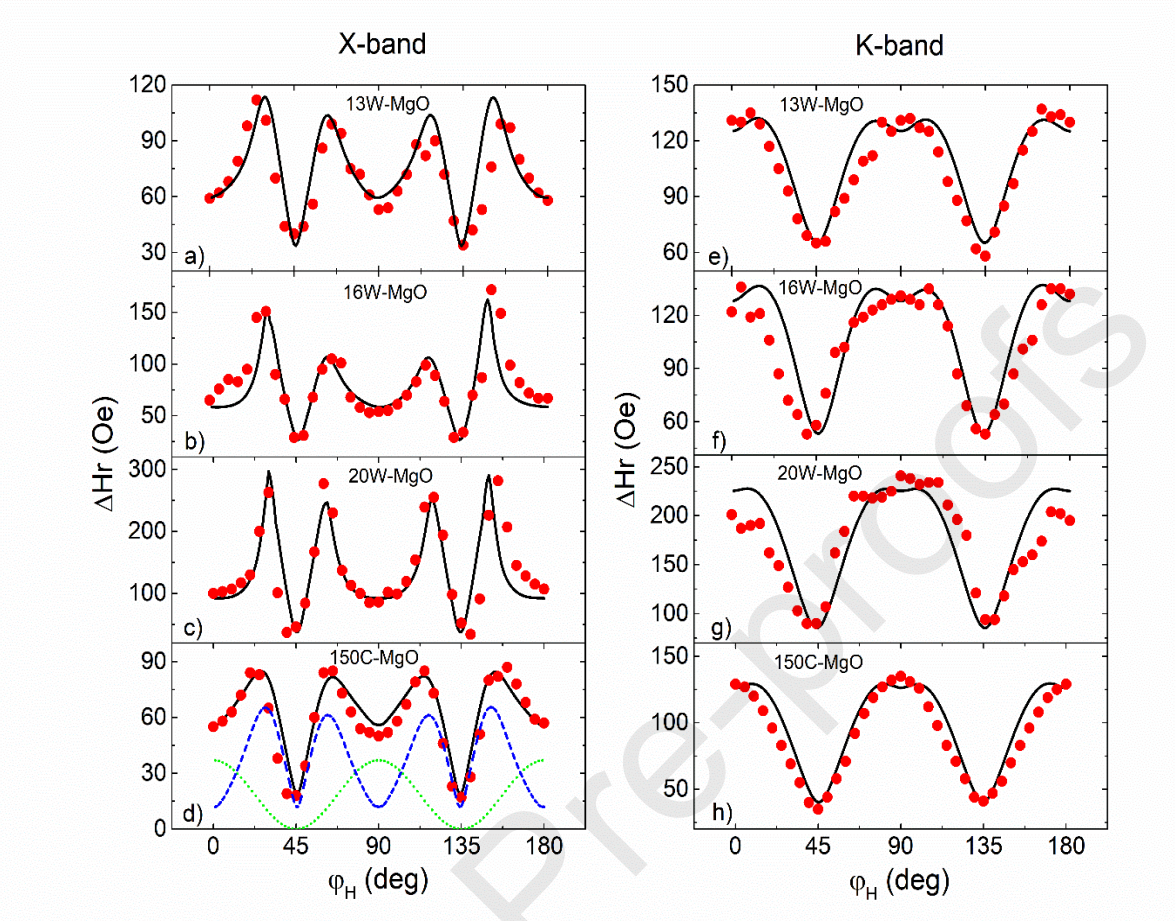

Fig. 5. Angular variation of ΔH_r (solid circles) and added contributions of ΔH_{2M} and mosaicity (solid lines) for X-band and K-band. In panel d) we also show the individual contribution of ΔH_{2M} and $\Delta\varphi_m$ as dotted and dashed lines, respectively.

Table IV. Values of α obtained from the fit of the frequency dependence of ΔH_r for the hard direction with Eq. (5) (Fig. 4(b)) and the simulated parameters $\Delta\varphi_m$ (mosaicity) and Γ^{ω}.

Sample	α	$\Delta\varphi_m$ (deg.)	Γ^{BX} (Oe)	Γ^{BK} (Oe)
13W-MgO	0.0045(1)	1.2(1)	26(1)	60(4)
16W-MgO	0.0047(1)	1.2(1)	32(2)	75(6)
20W-MgO	0.0055(1)	1.4(1)	57(6)	140(15)
150C-MgO	0.0030(1)	1.3(1)	37(3)	86(8)

The simulated curves in Fig. 5 describe very well the behavior of the angular variation of ΔH_r. The parameter $\Delta\varphi_m$ is of the order of those reported in systems with cubic anisotropy [**34-36**], furthermore, no significant variation is observed with the sputtering power. In order to verify that the proposed contributions are valid for other excitation frequencies, we also fitted the angular variation of ΔH_r measurements in W-band for the 150C-MgO sample using the same set of parameters used in Figs. 5(d) and 5(h), obtaining an very good agreement between model and experiment. (See Fig. S3(b) supplemental material). For the sample 150C-MgO the simulated values Γ^{BX} and Γ^{BK} extrapolate to $\Gamma{\sim}200$ Oe which agrees very well with the estimation made ($\Gamma = 195\ (20)$ Oe) using Eqs. (5) and (6) in the ΔH_r vs. ω dependence for this sample (dashed line in Fig. 4(a)). We can see that the Γ values obtained for samples 13W-MgO, 16W-MgO and 150C-MgO are similar. On the other hand, the value of Γ for the 20W sample is considerably higher which seems to be related to the higher concentration of structural defects, consistent with the greater coercive field that is seen in the hysteresis loops (Fig. 1(c)).

Conclusions

We have performed the magnetic characterization of Si (001) and MgO (001)/$Fe_{80}Co_{20}$(10 nm)/Ta (5 nm) bilayers with dynamic (FMR), magneto-optical (MOKE) and static (VSM) techniques. We have found that the optimal growth conditions to obtain a minimum in the damping constant and films with cubic symmetry are ~13-16 W of sputtering power and single crystal MgO substrates. Substrate heating during sputtering at temperatures of 150 ºC also helps to produce better quality films. The deposited samples on MgO show epitaxial growth with the axis [100] of the $Fe_{80}Co_{20}$ rotated by 45º from the axis [100] of the MgO substrate. We obtained damping parameters as low as $\alpha{\sim}3\times10^{-3}$ which are considerably smaller than those usually reported in ferromagnetic conductors ($\alpha \sim 10^{-2}$) and are in the range of values expected for this concentration, which makes these bilayers a good system for the injection of spin currents in spintronic applications. We made simulations to estimate the mosaicity and obtained relatively small values, consistent with a good quality of the deposited samples. We also estimated the strength of the two magnon scattering which agrees with values reported in Fe-rich alloys. Studies of the spin transport properties of these bilayers for potential applications in spintronic devices are presently being conducted.

Supplementary Material

See the supplementary material for details of x-ray diffraction and FMR W-band measurements.

Acknowledgements

Technical support from Rubén E. Benavides, César Pérez, and Matías Guillén is greatly acknowledged. This work was partially supported by Conicet under Grant PIP 201501-00213, ANPCyT Grant PICT 2013-0401, and U.N. Cuyo Grant 06/C556 all from Argentina. We also received financial support through the international cooperation project between Argentina and Belgium MINCyT-FWO FW/15/01 -VS.041.16N.

References

[1] K. Ando, Semicond. Sci. Technol. **29**, 043002 (2014).

[2] Y. Tserkovnyak, A. Brataas, and G. E. W. Bauer, Phys. Rev. Lett. **88**, 117601 (2002).

[3] E. Saitoh, M. Ueda, H. Miyajima, and G. Tatara, Appl. Phys. Lett. **88**, 182509 (2006).

[4] M. Tischer, O. Hjortstam, D. Arvanitis, J. Hunter Dunn, F. May, K. Baberschke, J. Trygg, J. M. Wills, B. Johansson, and O. Eriksson, Phys. Rev. Lett. 75, 1602 (1995).

[5] J. E. Gómez, B. Zerai Tedlla, N. R. Álvarez, G. Alejandro, E. Goovaerts, and A. Butera Phys. Rev. B **90**, 184401 (2014).

[6] A. Brataas, Y. Tserkovnyak, and G. E. W. Bauer, Phys. Rev. Lett. **101**, 037207 (2008).

[7] Y. Liu, A. A. Starikov, Z. Yuan, and P. J. Kelly, Phys. Rev. B **84**, 014412 (2011).

[8] S. Zhang, and Z. Li, Phys. Rev. Lett. **93**, 127204 (2004).

[9] E. M. Hankiewicz, G. Vignale, and Y. Tserkovnyak, Phys. Rev. B **78**, 020404 (2008).

[10] J. Gómez and A. Butera, Physica B **354**, 145 (2004).

[11] R. Arias and D.L. Mills, Phys. Rev. B **60**, 7395 (1999).

[12] M. J. Hurben and C. E. Patton, J. Appl. Phys. **83**, 4344 (1998).

[13] Kh. Zakeri, J. Lindner, I. Barsukov, R. Meckenstock, M. Farle, U. von Hörsten, H. Wende, W. Keune, J. Rocker, S. S. Kalarickal, K. Lenz, W. Kuch, and K. Baberschke, Phys. Rev. B **76**, 104416 (2007).

[14] Martin A.W. Schoen, Danny Thonig, Michael L. Schneider, T. J. Silva, Hans T. Nembach, Olle Eriksson, Olof Karis and Justin M. Shaw. Nature Physics, **12**, 839 (2016).

[15] Qing-feng Zhan, Chris Van Haesendonck, Stijn Vandezande, and Kristiaan Temst. Appl. Phys. Lett. **94**, 042504 (2009).

[16] W. Weber, R. Allenspach, and A. Bischof. Appl. Phys. Lett. **70**, 520 (1997).

[17] R. P. Cowburn, S. J. Gray, J. Ferré, J. A. C. Bland, and J. Miltat. J. Appl. Phys. **78**, 7210 (1995).

[18] Srijani Mallik, Niru Chowdhury, and Subhankar Bedanta. AIP Advances **4**, 097118 (2014).

[19] Qing-feng Zhan, Chris Van Haesendonck, Stijn Vandezande, and Kristiaan Temst. Appl. Phys. Lett. **91**, 122510 (2007).

[20] G. Couderchon and J. F. Tiers, Some aspects of magnetic properties of Ni-Fe and Co-Fe alloys, J. Magn. Magn. Mat., **26**, 196 (1982).

[21] M. Getzlaff, Fundamentals of Magnetism, ISBN 978-3-540-31150-8, (Springer-Verlag Berlin Heidelberg 2008).

[22] V.M. Pusenkov, K. Moskalev, N. Pleshanov, A. Schebetov,V. Syromyatnikov, V.Ul'yanov, A. Kobzev, O. Nikonov. Physica B **276**, 654 (2000).

[23] J. Smit and H. G. Beljers, Philips Res. Rep. **10**, 133 (1955).

[24] H. Kumar, D. R. Cornejo, S. L. Morelhao, S. Kycia, I. M. Montellano, N. R. Álvarez, G. Alejandro, and A. Butera, J. Appl. Phys. **124**, 085306 (2018).

[25] M. J. Jiménez, G. Cabeza, J.E. Gómez, D. Velázquez Rodriguez, L. Leiva, J. Milano, and A. Butera, J. Magn. Magn. Mat., **501**, 166361 (2020).

[26] N. R. Álvarez, J. E. Gómez, A. E. Moya Riffo, M. A. Vicente Álvarez, and A. Butera, J. Appl. Phys. **119**, 083906 (2016).

[27] N. Álvarez, G. Alejandro, J. Gómez, E. Goovaerts and A. Butera, J. Phys. D: Appl. Phys. **46**, 505001 (2013).

[28] S. Mizukami, D. Watanabe, M. Oogane, Y. Ando, Y. Miura, M. Shirai, and T. Miyazaki, J. Appl. Phys. **105**, 07D306 (2009).

[29] Yuelei Zhao, Qi Song, See-Hun Yang, Tang Su, Wei Yuan, Stuart S. P. Parkin, Jing Shi, and Wei Han, Sci. Rep-Uk. **6**, 22890 (2016).

[30] Isao Kanada, Alex Cruce, Tim Mewes, Shuang Wu, Claudia Mewes, Gary Mankey, and Takao Suzuki, AIP. Advances. **7**, 056105 (2017).

[31] C. Vittoria, S. D. Yoon and A. Widom, Phys Rev. B **81**, 014412 (2010).

[32] R. Meckenstock, D. Spoddig, Z. Frait, V. Kambersky and J. Pelzl, J. Magn. Magn. Mater. **272–276**, 1203 (2004).

[33] K. Lenz, H. Wende, W. Kuch, and K. Baberschke, Phys. Rev. B **73**, 144424 (2006).

[34] A. Butera, J.L. Weston, J.A. Barnard, J. Magn. Magn. Mat., **288**, 17 (2004).

[35] Yu V. Goryunov, N.N. Garifýanov, G.G. Khaliullin, I.A. Garifullin, L.R. Tagirov, F. Schreiber, Th. Mühge, H. Zabel, Phys. Rev. B **52**, 13450 (1995).

[36] J.R. Fermin, A. Azevedo, F.M. de Aguiar, B. Li, S.M. Rezende, J. Appl. Phys. **85**, 7316 (1999).

D. Velázquez Rodriguez: Methodology, Formal analysis, Writing - Original Draft, Investigation, Software, Writing - Review & Editing

J. E. Gómez: Methodology, Formal analysis, Investigation, Writing - Review & Editing

G. Alejandro: Investigation, Writing - Review & Editing

L. Avilés Félix: Methodology, Investigation, Writing - Review & Editing

M. van Landeghem: Investigation, Writing - Review & Editing

E. Goovaerts: Conceptualization, Methodology, Formal analysis, Writing - Review & Editing

A. Butera: Conceptualization, Methodology, Formal analysis, Investigation, Writing - Review & Editing, Supervision, Project administration, Funding acquisition

Declaration of interests

☒ The authors declare that they have no known competing financial interests or personal relationships that could have appeared to influence the work reported in this paper.

☐The authors declare the following financial interests/personal relationships which may be considered as potential competing interests:

-We performed an experimental research on the magnetic properties of $Fe_{80}Co_{20}$ thin films of varying sputtering conditions (sputtering power and temperature) on MgO (001) and Si (001) substrates.

-We have determined the optimum sputtering conditions to obtain ultra-low damping values of the constant α ($\leq 10^{-3}$), crucial for future applications in spintronic devices.

-We have found that using the optimum sputtering conditions the films grow epitaxially on MgO single crystal substrates.

-We have performed an exhaustive study of the dynamic response of the magnetization. To analyze the relaxation mechanism, we made computer simulations considering the intrinsic Gilbert damping, the extrinsic two magnon scattering and mosaicity contributions, finding and excellent agreement between the model and the experimental data.